BIOCHEMISTRY
including biophysical chemistry & molecular biology

Article

pubs.acs.org/biochemistry

Peptide Amyloid Surface Display

Marisa A. Rubio, Diana E. Schlamadinger, Ellen M. White, and Andrew D. Miranker*

Department of Molecular Biophysics and Biochemistry, Yale University, 260 Whitney Avenue, New Haven, Connecticut 06520-8114, United States

Supporting Information

ABSTRACT: Homomeric self-assembly of peptides into amyloid fibers is a feature of many diseases. A central role has been suggested for the lateral fiber surface affecting gains of toxic function. To investigate this, a protein scaffold that presents a discrete, parallel β-sheet surface for amyloid subdomains up to eight residues in length has been designed. Scaffolds that present the fiber surface of islet amyloid polypeptide (IAPP) were prepared. The designs show sequence-specific surface effects apparent in that they gain the capacity to attenuate rates of IAPP self-assembly in solution and affect IAPP-induced toxicity in insulin-secreting cells.

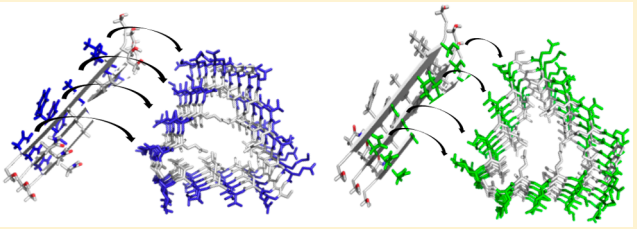

The spontaneous conversion of soluble protein to β-sheet rich filaments is a basic property of polypeptides.[1] These filaments, termed amyloid fibers, are defined by their histologic staining characteristics and structural properties. The latter includes β-sheet in which the sheets run in the direction of the filaments while the strands run orthogonal to the long filament axis. This cross-β structure tends to be highly stable and irreversible. Naturally occurring proteins have largely evolved sequences that avoid the formation of such states. Notable exceptions to this occur, for example, in PMEL17 which is a filamentous protein that stabilizes the pigment melanin.[2] There, the long-term stability of protein in dead tissue is desirable for this structural scaffold.

In many diseases, conversion to amyloid either causes or significantly contributes to disease pathology.[3] These include neurodegenerative diseases, such as Alzheimer's and Parkinson's, but also diseases as diverse as HIV/AIDS and cancer.[4,5] Recent structural insights into these diseases have mapped the initiation of pathology to the self-assembly of short segments within a larger polypeptide, lending credence to the study of short amyloidogenic peptides.[6] A particularly engaging example is the gain of dominant negative phenotype in many cancers. Specifically, many forms of mutated p53 (a tumor suppressor) result in loss of function not only of the mutated p53 but also of heterozygously expressed wild-type p53. This property was mapped to the self-assembly of a computationally predicted seven-residue segment buried within the 393-amino acid protein. The mutated p53 is structurally destabilized, exposing the aggregation-prone segment, resulting in co-aggregation with wild-type p53 as well as paralogs p67 and p73.[3,5]

p53 highlights a fundamental aspect of amyloid kinetics, namely, a separation of nucleation and elongation phenomena. Nucleation itself can be further divided into two components. Primary nucleation is the formation of new fiber ends from precursor material. Secondary nucleation is the formation of new fiber ends that is dependent on the presence of preexisting fiber. A simple example of the latter is fiber breakage. More intriguing, however, is the presence of secondary processes that are dependent on both fiber and precursor. In this case, the walls of amyloid fibers likely serve as sites for template-assisted formation of new fibers and/or prefibrillar intermediates.[4,5,7,8] We have previously shown kinetically that this phenomenon takes place with a 10-residue peptide subdomain of islet amyloid polypeptide (IAPP), $IAPP_{20-29}$.[7] More recently, the phenomenon of surface-based secondary nucleation has become biomedically relevant. For Aβ in Alzheimer's and IAPP in type II diabetes, we and others have observed that secondary nucleation can be an origin of cytotoxic gains of function.[8,9]

Investigation of secondary nucleation phenomena is challenged by the complex reaction landscape of amyloid formation. Fiber formation follows a sigmoidal reaction profile with primary nucleation followed by elongation. Once sufficient elongation has occurred, secondary nucleation processes become dominant over primary and the rate of new fiber formation and elongation becomes overwhelming. The capacity of these reactions to be accelerated by seeding with preexisting fibers is an important defining characteristic of nucleation-dependent kinetics.[10] For $IAPP_{20-29}$ and Aβ, it has been shown (and is therefore possibly generalizable) that such secondary nucleation processes are both monomer- and fiber-dependent. The former requires contributions to secondary nucleation that are not the direct result of fiber fragmentation.[7,8] This was a surprising finding, in part, as branching in amyloid is seldom directly observed by electron microscopy (EM). Rather, the frequent presence of unresolvable fiber clumping by EM is thought to be the result of a high degree of nucleation proximal to preexisting fibers. Regardless, flat lag phases and the

Received: September 10, 2014
Revised: December 22, 2014
Published: December 26, 2014

ACS Publications © 2014 American Chemical Society

DOI: 10.1021/bi5011442
Biochemistry 2015, 54, 987−993

retention of sigmoidal profiles in seeded kinetics are qualitative hallmarks of the presence of secondary nucleation.

In this work, we show the importance of surface specificity to nucleation using the system $IAPP_{20-29}$ and the parent, wild-type protein IAPP. We achieve this by engineering a generalizable protein template scaffold that can support studies of non-fragmentation-based secondary nucleation in any peptide system. The protein design is meant to address a critical issue, namely creation of a surface capable of secondary nucleation without being subject to elongation. Finally, we show that the designed scaffolds interact with full-length IAPP and are capable of rescuing IAPP toxicity toward cells.

MATERIALS AND METHODS

Materials. Potassium chloride, potassium phosphate salts, and DMSO were purchased from J. T. Baker (Phillipsburg, NJ), and thioflavin T (ThT) was purchased from Acros (Geel, Belgium). Synthetic $IAPP_{20-29}$ was purchased from the W. M. Keck Foundation Biotechnology Resource Laboratory (Yale University) and GenScript Corp. (Piscataway, NJ) at >98% purity. The stock was dissolved in 30% acetonitrile, split into aliquots, lyophilized, and stored at −80 °C. Peptides were dissolved in DMSO to a concentration of 7.5 mM and used immediately in kinetic experiments. The concentration of stock solutions was determined by one-dimensional ^{1}H NMR, comparing the integrated areas of peaks from phenylalanine aromatic protons with a known concentration TMS standard introduced into the sample.

Synthetic full-length human IAPP was purchased from Elim Biopharmaceuticals (Hayward, CA). Protein stocks were generated as described previously with the use of a 50% acetonitrile/0.2% formic acid mixture as the eluent from a MacroSpin column (The Nest Group, Southborough, MA).[11] This stock was split into aliquots, lyophilized, and stored at −80 °C. Aliquots were dissolved with water to a concentration of 1 mM and used immediately in cell-based experiments.

The gp5-$(His)_6$ gene was a gift from S. Kanamaru (Tokyo Institute of Technology, Tokyo, Japan). The $gp5_{\beta f}$ portion of gp5 was subcloned into a pJexpress 414 plasmid containing the foldon gene, purchased from DNA2.0, Inc. (Menlo Park, CA). Genes of $gp5_{NGIS}$ and $gp5_{NFAL}$ with N-terminal $(His)_6$ tags in the pJ414 vector were also purchased from DNA2.0, Inc. Expression and purification of $gp5_{\beta f}$ proteins followed a modified protocol received with the gp5-$(His)_6$ gene. Gp5 proteins were purified by affinity chromatography using Ni-NTA resin (Qiagen) and by gel filtration chromatography using Superdex 200 resin (GE Healthcare Life Sciences).

Fiber Formation Reactions and Kinetics. Reactions of $IAPP_{20-29}$ were initiated by diluting 7.5 mM peptide stocks into 100 mM KCl, 50 mM potassium phosphate buffer (pH 7.4). $IAPP_{20-29}$ kinetics in a quiescent solution were monitored by 90° light scatter. Light scatter was monitored using a dual-emission PTI QuantaMaster C-61 fluorescence spectrometer using excitation and emission wavelengths of 400 nm. IAPP reactions were monitored by ThT; 200 nM ThT was premixed with the aqueous component of the reaction mixtures prior to the addition of peptide. Reactions were conducted in a Microfluor black 96-well plate (Thermo Electron) in volumes of 25−100 μL. Fluorescence was monitored in a FluoDia T70 plate reader (PTI) using bandpass filters at 425 and 486 nm for excitation and emission, respectively.

Reaction t_{50} values were determined by fitting to the following equation:

$$f(t) = (m_1 t + r_1)\left(\frac{1}{1 + e^{t_{50}-t/\tau}}\right) + (m_2 t + r_2)\left(1 - \frac{1}{1 + e^{t_{50}-t/\tau}}\right)$$

where $f(t)$ is the scatter or fluorescence intensity and m_1, m_2, r_1, r_2, τ, and t_{50} are constants determined by the fit, where m_1 and m_2 are the slopes of the upper and lower baselines, respectively, r_1 and r_2 are the y values of the upper and lower baselines, respectively, and τ describes the degree of cooperativity/sharpness of the sigmoid function. Data points were collected every 120 s and all fits were performed on raw data. Reported errors are standard deviations from at least three independent measurements. Data shown in figures are box averaged with a window of five points.

HPLC. End-stage kinetic reaction mixtures were spun down (14000*g* for 10 min), and the supernatant was applied to a Vydac reverse-phase analytical C18 column (Grace, Columbia, MD). Peak areas from elution profiles were integrated using Origin 8.2.

Size Exclusion Chromatography. End-stage kinetic reaction mixtures were spun down (14000*g* for 10 min), and the supernatant was applied to a Superdex 200 column with a 25 mL resin bed equilibrated with 20 mM Tris-HCl, 0.1 M NaCl, and 10 mM EDTA (pH 7.9) at 4 °C. Peak areas were integrated using Origin 8.2.

Transmission Electron Microscopy. Supernatants of samples after centrifugation (14000*g* for 10 min) were applied directly to carbon-coated copper grids (Electron Microscopy Sciences). A 5 μL sample was applied to grids and after 1 min, the grids were washed with water and stained with 0.5% uranyl acetate (pH 4.4). Images were taken using a Zeiss EM 900 microscope (50 kV accelerating voltage) that is equipped with an Olympus SIS Megaview 3 CCD.

Cell Toxicity Assays. Rat insulinoma INS-1 cells (832/13, G. W. Cline, Department of Internal Medicine, Yale University) were cultured at 37 °C and 5% CO_2 in phenol red free RPMI 1640 medium supplemented with 10% fetal bovine serum, 1% penicillin/streptomycin (all from Life Technologies, Carlsbad, CA), and a 2% INS-1 stock solution [0.5 M HEPES, 100 mM L-glutamine, 100 mM sodium pyruvate, and 2.5 mM β-mercaptoethanol (all from Sigma-Aldrich, St. Louis, MO)]. Cells were passaged upon reaching ∼95% confluence (0.25% trypsin-EDTA, Life Technologies), propagated, and/or used in experiments. Cells used in experiments were pelleted and resuspended in fresh medium with no trypsin-EDTA.

Cell viability was measured using the Cell-Titer Blue (CTB) fluorescence-based assay. CTB reagent (Promega, Madison, WI) comprises nonfluorescent resazurin, which is metabolically reduced to fluorescent resorufin in living cells. Cells were plated at a density of 20000 cells/well (500 μL/well) in 24-well plates (BD Biosciences, San Diego, CA). After the cells had been cultured for 48 h, medium was replaced with fresh medium containing human IAPP and $gp5_{\beta f}$ premixed at the desired concentration. Cells were incubated at 37 °C and 5% CO_2 with peptide and $gp5_{\beta f}$ proteins for an additional 48 h. After the incubation period, CTB reagent (100 μL) was added to each well and incubated at 37 °C and 5% CO_2 for 3−3.5 h. The fluorescence of the resorufin product was measured on a FluoDia T70 fluorescence plate reader (Photon Technology International, Birmingham, NJ). All solutions included 0.16% 10 mM KCl, 5 mM potassium phosphate (pH 7.4), and 0.65%

DOI: 10.1021/bi5011442
Biochemistry 2015, 54, 987−993

H_2O to account for the addition of $gp5_{\beta f}$ and IAPP vehicle to sample wells. Wells that included vehicle but not peptide or $gp5_{\beta f}$ served as the negative control (100% viable), and wells containing 10% DMSO were the positive control (0% viable). The percent toxicity was calculated using the following equation:

$$\%\ \text{toxicity} = 100 - 100\left(\frac{\langle S\rangle - \langle P\rangle}{\langle N\rangle - \langle P\rangle}\right)$$

Each independent variable is the average fluorescence of three technical replicates from the negative control ($\langle N\rangle$), positive control ($\langle P\rangle$), and samples ($\langle S\rangle$) or two technical replicates for $gp5_{\beta f}$ only. Data presented in Figure 5 are the average of three independent experiments.

RESULTS AND DISCUSSION

Surface-Mediated Primary Nucleation. Primary Nucleation Can Be Blocked. In earlier work, we showed that apparent secondary nucleation processes in $IAPP_{20-29}$ shared a common reaction order and Arrhenius behavior with primary nucleation.[7] This coincidence led us to suggest that secondary nucleation, at least in this system, is simply a manifestation of surface-catalyzed primary nucleation. Here, we have sought to test this hypothesis by blocking the unavoidable presence of solid contaminants that can serve as nucleating surfaces. Fiber formation reactions of $IAPP_{20-29}$ are initiated by dilution of DMSO peptide stock solutions into aqueous buffer. Solutions are then monitored over time for changes in 90° light scatter. The observed reaction midpoints, t_{50}, at 750 μM $IAPP_{20-29}$ are 5500 ± 1500 s, consistent with our earlier work.[7] Remarkably, as little as 10 nM BSA, a 75000:1 substoichiometric ratio, present as the reaction is initiated inhibits fiber formation beyond our measurement time of 10 h. This effect is dose-dependent with 1 and 3 nM BSA extending t_{50} to 7500 ± 1800 and 12000 ± 2100 s, respectively (Figure 1A). At face value, BSA appears to be an extraordinary, substoichiometric inhibitor of amyloid assembly.

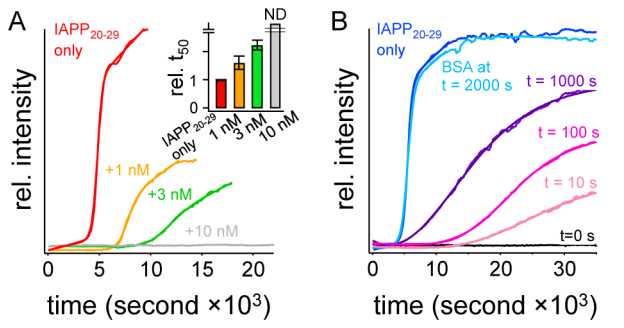

Figure 1. Fiber formation can be blocked by BSA. (A) A representative 750 μM standard $IAPP_{20-29}$ reaction is initiated by dilution of a DMSO stock solution of $IAPP_{20-29}$ into buffer and monitored by orthogonal light scatter (red). Matched reactions are shown with addition of 1 nM (orange), 3 nM (green), or 10 nM (gray) BSA. The inset shows statistics of relative reaction midpoints, t_{50}, from at least three repeats of data such as in panel A. (B) Representative data for time-dependent inhibition of 750 μM $IAPP_{20-29}$ assembly by 10 nM BSA. BSA was either not added (blue) or added to reaction mixtures at the indicated times after reaction initiation. ND in the inset of panel A indicates no detected change after observation for 10 h.

Inhibition of $IAPP_{20-29}$ Assembly Is Dependent on the Time of BSA Addition. BSA (10 nM) added 2000 s after the parent assembly reaction is initiated no longer displays inhibition (Figure 1B). Reactions were then conducted such that BSA was added at time points within the lag phase of an $IAPP_{20-29}$-only reaction. BSA added at later time points shows a progressive shortening of t_{50} (Figure 1B). Nonspecific blocking is a well-known, general phenomenon of BSA. It is likely that BSA is blocking sites at which nucleation can take place. A similar effect has been observed for Aβ, in which human serum albumin was shown to be capable of inhibiting Aβ self-assembly.[12,13] Indeed, in IAPP and Aβ, exceptionally robust, reproducible kinetics are achievable provided scrupulous efforts are made to remove preexisting aggregates.[7,14] The presence of a new fiber surface then dictates all downstream aspects of amyloid kinetics. Contaminating surfaces are relevant to primary nucleation, and low concentrations of initial fibers are responsible for apparent secondary nucleation and elongation phases of amyloid assembly. It is likely that secondary nucleation occurs through sequence-specific interactions of the protein with walls of existing fibers. Any effort to understand the role of secondary nucleation will therefore require separate control of surface and fiber end elements of the reaction.

Surface Design. We seek to isolate surface contributions to secondary nucleation by designing protein templates that display the residues that are found on the $IAPP_{20-29}$ fiber surface without displaying $IAPP_{20-29}$ fiber ends. $IAPP_{20-29}$ is capable of adopting parallel or antiparallel β-strand assemblies in its zwitterionic state.[15] We have previously shown using electron paramagnetic resonance that the C-terminally amidated $IAPP_{20-29}$ stacks as an in-register parallel β-sheet.[16] In this work, the amidated form of $IAPP_{20-29}$ is used to ensure parallel assembly in keeping with the nature of full-length IAPP.[17] Others have shown that amyloidogenicity of SNNFGAILSS can be further reduced to a six-residue core, NFGAIL.[18,19] Thus, individual parallel β-sheets of $IAPP_{20-29}$ fibers can be described, in part, as NxGxIxS residues displayed on one side of a β-sheet and NxFxAxL on the other (panels C and D of Figure 2, respectively). In our own work with amidated $IAPP_{20-29}$, it is not clear if intersheet interactions occur in a head-to-head (NGIS facing NGIS) or head-to-tail (NGIS facing NFAL) fashion. Regardless, it is reasonable to assume that a fiber wall formed from $IAPP_{20-29}$ displays along its entire length a residue stack of NxGxIxS, NxFxAxL, or both. It is this surface that may provide the nucleation site for precursor-dependent secondary nucleation.

The homotrimeric gene product (gp)5−gp27 protein complex functions as the baseplate hub and cell-puncturing device of bacteriophage T4 (Figure 2A).[20] Gp5 contains a long, solvent-exposed, β-helix portion that displays parallel stacks of six-residue β-strands separated by two-residue turns. This β-solenoid subdomain with 18 winds can be separated from the intact gp5 lysozyme domain while still maintaining its fold.[21] Previous work has shown that a fragment of the gp5 β-helix can be expressed in isolation and independently crystallized for atomic structure determination.[22] This fragment, $(gp5_{\beta f})_3$, here simply termed $gp5_{\beta f}$, consists of the 85 C-terminal residues of the β-helix fused to a flexible linker and a self-trimerizing, 27-residue β-propeller subunit at the C-terminus (Figure 2B). This β-propeller, termed foldon, assists in assembly of the homotrimer and robustly caps one of the ends.[23] The gp5 structure has unique merit for our study of the β-helix. Namely,

DOI: 10.1021/bi5011442
Biochemistry 2015, 54, 987−993

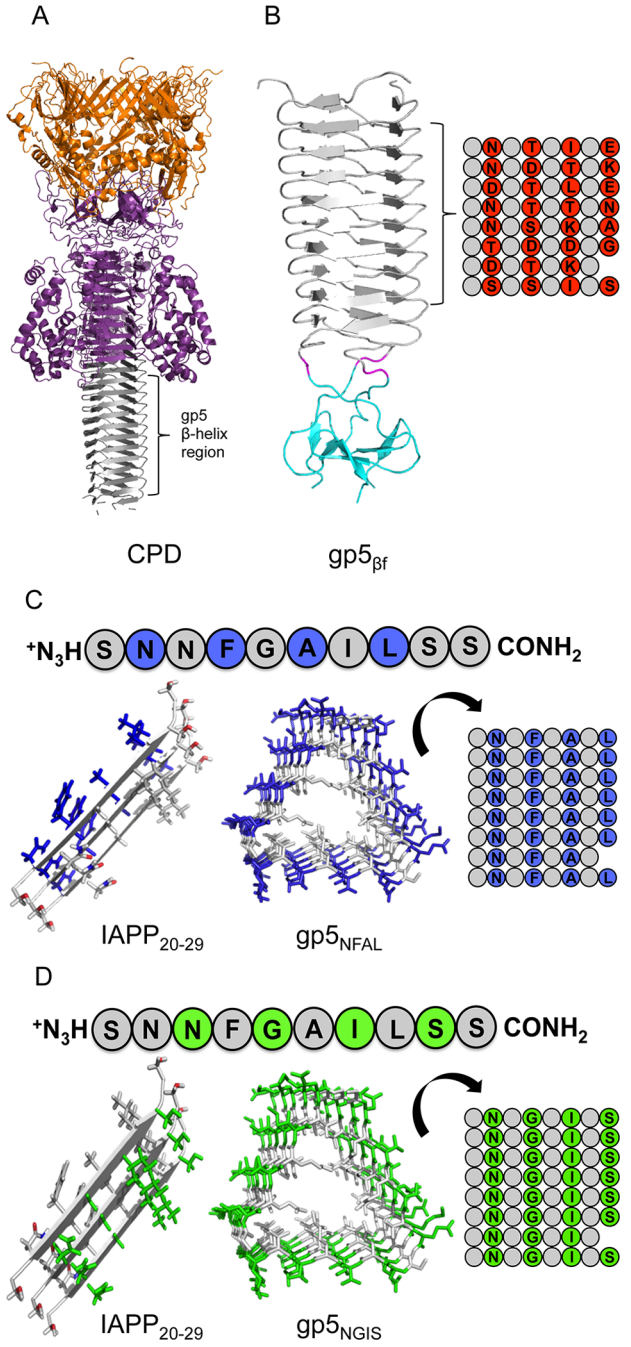

Figure 2. Schematic of protein template design. (A) Cell-puncturing device from T4 phage λ (Protein Data Bank entry 1K28).[20] (B) $gp5_{\beta f}$ base structure derivatized in this work. The foldon domain is colored cyan, the linker magenta, and the C-terminal β-helix region from panel A gray (Protein Data Bank entry 3A1M).[22] Native residues with exposed side chains are shown as red circles with one-letter amino acid code, and inward-pointing residues are shown as gray circles. (C and D) The sequence of $IAPP_{20-29}$ used in this work is shown at the top of each panel, with a three-strand canonical parallel β-sheet shown at the left. Residues of NFAL (C, blue) and NGIS (D, green) from $IAPP_{20-29}$ at the left are shown at the matched positions of a subset of the β-solenoid winds of panel B.

each of the three homologous faces of the helix can present a solvent-exposed series of residues (i, i + 2, i + 4, and i + 6) without impacting the core residues that stabilize the $gp5_{\beta f}$ structure.

A uniform population of putative amyloid fiber wall mimics, eight stacked β-strands long, can be created on each of the three faces of this scaffold. For $IAPP_{20-29}$, the four exterior residues of each of these β-strands were mutated to uniformly display either NxGxIxS ($gp5_{NGIS}$) or NxFxAxL ($gp5_{NFAL}$) on each of the three faces with the exception of the seventh β-strand, which does not contain a fourth position (Figure 2C,D). As residue changes are in 100% solvent-exposed and non-interacting positions, no change was expected or observed in the overall structure of the designed $gp5_{\beta f}$ templates (Figure S1 of the Supporting Information).

Validation. Sigmoidal kinetic assembly of $IAPP_{20-29}$ is lost when the process is conducted in the presence of $gp5_{\beta f}$. A 750 μM $IAPP_{20-29}$ standard fiber formation reaction was conducted alone or in buffer containing 10 μM parent protein $gp5_{\beta f}$. The nucleation-dependent profile of the former is plainly absent in the latter (Figure 3). Instead, light scatter is apparent within the

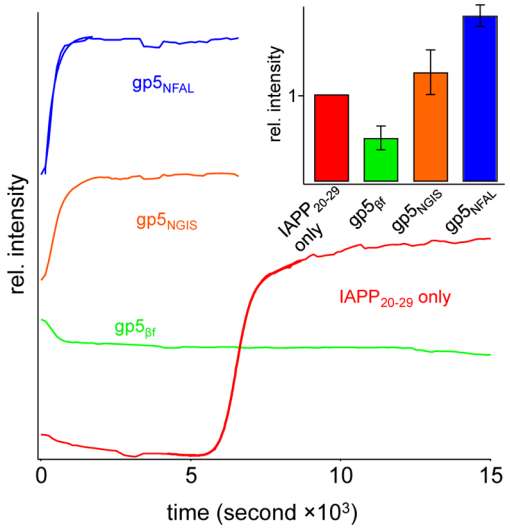

Figure 3. Effect of $gp5_{\beta f}$ structures on the kinetic assembly of $IAPP_{20-29}$ monitored by 90° light scatter. Shown is the addition of 10 μM $gp5_{NFAL}$ (blue), $gp5_{NGIS}$ (orange), or $gp5_{\beta f}$ (green) to a 750 μM $IAPP_{20-29}$ assembly reaction mixture. The profile of the $IAPP_{20-29}$-only reaction is colored red. The inset shows the statistics of the final scatter intensity from repeated independent trials.

dead time of measurement (~2 min). The magnitude of this scatter is reproducible at 0.5 ± 0.1 the intensity of the $IAPP_{20-29}$-only reaction. Further changes to the kinetic profile are mostly absent. This may reflect strong acceleration of the amyloid reaction or formation of a non-amyloid aggregate species that may be on or off the amyloid assembly pathway. In any case, the assembly of $IAPP_{20-29}$ is plainly affected by the presence of this β-solenoid at a stoichiometry of 75:1.

The kinetic profile of designed $gp5_{\beta f}$-affected $IAPP_{20-29}$ assembly displays sequence dependence. $IAPP_{20-29}$ reactions were conducted in the presence of 10 μM $gp5_{NGIS}$ or $gp5_{NFAL}$ (Figure 3). As with $gp5_{\beta f}$, light scatter is apparent in the dead time of measurement. In contrast, however, is the presence of an additional kinetic component, giving rise to light scatter contributions that are larger than that of $IAPP_{20-29}$ alone. The magnitude of the ending light scatter is reproducible and greater for $gp5_{NFAL}$ (1.9 ± 0.1 the intensity of the $IAPP_{20-29}$) than for $gp5_{NGIS}$ (1.2 ± 0.2 the intensity of the $IAPP_{20-29}$) (Figure 3, inset). Fitting single-exponential curves to the rise in scatter gives similar time constants of 410 ± 40 and 360 ± 80 s

DOI: 10.1021/bi5011442
Biochemistry 2015, 54, 987−993

for $gp5_{NGIS}$ and $gp5_{NFAL}$, respectively. These rates are not significantly affected in reactions conducted instead at 1 and 25 μM $gp5_{\beta f}$ (not shown). Overall, the designed $gp5_{\beta f}$ templates are clearly interacting with $IAPP_{20-29}$, affecting assembly in a manner that is dependent upon which residues are displayed on the $gp5_{\beta f}$ surface. The parent $gp5_{\beta f}$ scaffold catalyzes aggregate formation to a lesser extent than the sequence-specific designed scaffolds. This suggests that the $IAPP_{20-29}$ peptide and $gp5_{\beta f}$ interface can also form through nonspecific interactions. This may be sufficient to increase the local concentration of $IAPP_{20-29}$, resulting in aggregation. Importantly, the sequence-specific designs rapidly catalyze formation of this aggregate to a much greater extent than the parent, wild-type $gp5_{\beta f}$.

Aggregates formed in the presence of β-solenoid peptide templates are small and soluble and contain amounts of template that are sequence-dependent. $IAPP_{20-29}$ fibers are pelleted at 14000*g*, eliminating all apparent scatter. In contrast, the light scattering aggregates formed in the presence of $gp5_{\beta f}$ proteins do not visibly pellet at 14000*g* (not shown). The magnitude of right angle light scatter is dependent on the size and concentration of the scattering species. Therefore, the concentration of soluble β-solenoid $gp5_{\beta f}$ in reaction supernatants was determined by reverse-phase HPLC with profiles integrated and compared to those of purified standards (Figure S2A of the Supporting Information). In mixed reactions, the parent sequence, $gp5_{\beta\beta}$, is distinctly more pelletable than $gp5_{NGIS}$ and $gp5_{NFAL}$, with 43 ± 11, 74 ± 3, and 87 ± 6% of β-solenoid $gp5_{\beta f}$ proteins remaining in the supernatant, respectively (Figure S2B of the Supporting Information). The components remaining in these supernatants were directly evaluated by size exclusion chromatography with detection at 280 nm. At this wavelength, the absorbance is overwhelmingly dominated by the 12 tryptophans of the β-solenoid molecules. We assume that it is the void volume fractions that contain the light scattering soluble aggregates (Figure S3A of the Supporting Information). For $gp5_{\beta f}$-containing reaction mixtures, the soluble aggregate contains 1 ± 0.2% of detectable β-solenoid. In contrast, 7 ± 3 and 9 ± 3% are apparent in reactions using $gp5_{NGIS}$ and $gp5_{NFAL}$, respectively (Figure S3B of the Supporting Information). Clearly, there is a quantitative difference in the capacity of $gp5_{\beta f}$ and $gp5_{NFAL}$ and $gp5_{NGIS}$ scaffolds to form soluble aggregates in reactions with $IAPP_{20-29}$.

Aggregates formed in mixed $IAPP_{20-29}/gp5_{\beta\beta}$, $IAPP_{20-29}/gp5_{NGIS}$, and $IAPP_{20-29}/gp5_{NFAL}$ reactions are not amyloid. Negative stain transmission electron microscopy shows $IAPP_{20-29}$-only reactions form well-defined filamentous amyloid as described previously (Figure 4A).[7] In contrast, mixed reactions show only heterogeneously sized (25−100 nm) amorphous species. No fibers were evident across many grids (Figure 4B−D). As it is possible the amorphous species are simply small sets of short amyloid segments, aggregates were also assayed using the amyloid indicator dye, ThT.[7] Using 10 μM ThT, $IAPP_{20-29}$ fibers give a strong response at 480 nm over protein-free ThT in buffer (Figure 4E). In mixed reactions using 750 μM $IAPP_{20-29}$ and 10 μM $gp5_{\beta f}$ proteins, no significant enhancement of fluorescence is observed over background. Plainly, the aggregates formed in mixed reactions are structurally distinct from $IAPP_{20-29}$ fibers.

Cell Toxicity. Secondary amyloid nucleation processes that are dependent on both fiber and precursor have been suggested as potential origins for so-called toxic oligomer formation in IAPP and Aβ.[8,9,24] Moreover, the outer surface of fibers of full-length IAPP likely displays part or all of the $IAPP_{20-29}$ subpeptide sequence as an oligomeric, in-register, parallel stack of $IAPP_{20-29}$ sequences.[25,26] We therefore assessed the capacity of $gp5_{\beta\beta}$, $gp5_{NGIS}$, and $gp5_{NFAL}$ to affect kinetic assembly profiles of wild-type IAPP in solution and to affect IAPP-induced cytotoxicity.

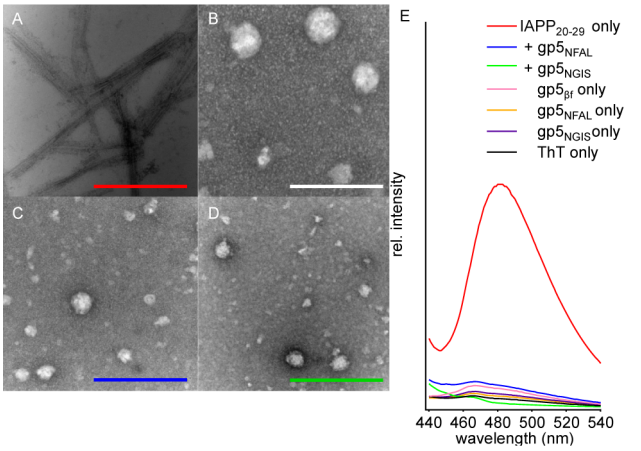

Figure 4. Morphological characterization of $gp5_{\beta f}$-affected assembly of $IAPP_{20-29}$. Negative stain TEM of fibers formed by 750 μM $IAPP_{20-29}$ alone (A). (B−D) The same reaction as in panel A, but with the addition of 10 μM $gp5_{\beta f}$ (B), $gp5_{NGIS}$ (C), or $gp5_{NFAL}$ (D). Reaction mixtures were incubated for ∼10 h before being analyzed. Scale bars are 200 nm. (E) Fluorescence emmission spectra of 10 μM ThT added to end-state $IAPP_{20-29}$ reactions of $IAPP_{20-29}$ alone (red) or in the presence of $gp5_{NFAL}$ (blue) and $gp5_{NGIS}$ (green). Data for ThT alone (black) or ThT added to buffer containing only 10 μM $gp5_{\beta f}$ (pink), $gp5_{NFAL}$ (orange), or $gp5_{NGIS}$ (purple) are also shown.

β-Solenoid scaffolds displaying IAPP sequence have a marked effect on wild-type IAPP assembly. Under the conditions presented here, 50 μM full-length human IAPP undergoes a transition to amyloid fiber with a t_{50} of 16000 ± 770 s (Figure 5A), assembling into amyloid more aggressively than $IAPP_{20-29}$. Remarkably, addition of as little as 100 nM $gp5_{NFAL}$ or $gp5_{NGIS}$ extinguishes amyloid assembly (total measurement time of ∼58000 s). In contrast, addition of 100 nM $gp5_{\beta f}$ increases t_{50} by a factor of only 1.7 ± 0.3. All three $gp5_{\beta f}$ structures show dose dependence (Figure 5B), suggesting that all three can display the observed effect on IAPP, albeit at different concentrations. Plainly, the $IAPP_{20-29}$ segment presented on the walls of the $gp5_{\beta f}$ proteins can manipulate, in this case inhibit, full-length IAPP aggregation kinetics.

Amyloid surface-presenting templates affect IAPP-induced toxicity. Wild-type IAPP is routinely shown to be toxic toward INS-1 cells, an immortal, insulin-secreting β-cell line by cell titer blue (CTB) and mitochondrial reductase activity (MTT) assays as well as by Western blotting and Alamar blue reduction assays.[11,27,28] Lot-to-lot variation of IAPP requires that we first assess toxicity by dose response to establish a standard concentration that achieves ∼50% toxicity in 48 h. Here, 13 μM IAPP results in 48 ± 2% toxicity averaged across three independent repeats of experiments containing two or three technical replicates each (Figure 5C). Parallel assessments in which 13 μM IAPP and 0.5 μM $gp5_{\beta f}$ are co-introduced into the culture media show no change in full-length IAPP toxicity. In contrast, 0.5 μM $gp5_{NGIS}$ or $gp5_{NFAL}$ showed a significant capacity to rescue cells from IAPP toxicity, with toxicity reduced to 32 ± 4 or 30 ± 5%, respectively. Note, at 0.5 μM, neither $gp5_{\beta\beta}$, $gp5_{NFAL}$, nor $gp5_{NGIS}$ displays any intrinsic

DOI: 10.1021/bi5011442
Biochemistry 2015, 54, 987−993

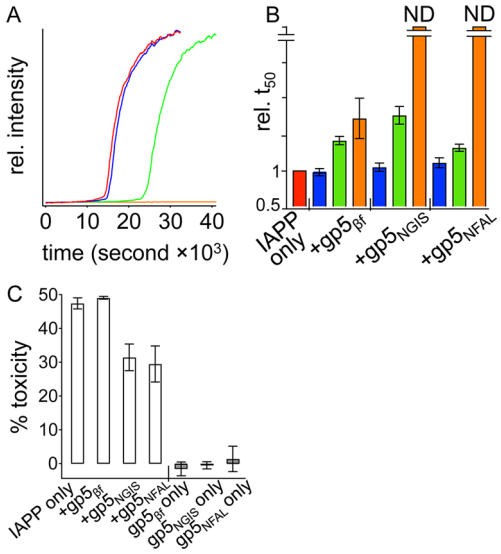

Figure 5. Interaction of $gp5_{\beta f}$ proteins with full-length, wild-type IAPP. (A) Data for a representative fiber formation reaction, monitored using fluorescence of 200 nM ThT, are shown with addition of 1 nM (blue), 10 nM (green), or 100 nM (orange) $gp5_{NGIS}$ to 50 μM IAPP. Data for the IAPP-only reaction are colored red. (B) Statistics of reaction midpoints, t_{50}, relative to IAPP-only t_{50} (red) from fits to repeats of kinetic measurements such as in panel A, but using the indicated $gp5_{\beta f}$ variant. (C) Toxicity of IAPP toward INS-1 cells at 13 μM IAPP alone and with the indicated $gp5_{\beta f}$ molecule at 0.5 μM (white bars). The toxicities of the indicated $gp5_{\beta f}$ proteins alone at 0.5 μM are shown as gray bars. ND in panel B indicates no detected change after observation for 16 h.

toxicity (Figure 5C). This suggests that IAPP subsequences on the surfaces of $gp5_{\beta f}$-based scaffolds specifically interact with elements of the parent IAPP sequence relevant to formation of toxic species. Alternatively, it is possible that the sequence-specific $gp5_{\beta f}$ designs are stabilizing and sequestering IAPP in a nontoxic state.

CONCLUSIONS

In this work, we have taken the first step toward the development of a uniform, small, and monodisperse representation of a peptide amyloid surface. The importance of surface control was demonstrated by showing the capacity of an oft-used surface-blocking agent, BSA, to arrest fiber formation. Throughout the amyloid literature, variations in reaction timescale from group to group and even within groups are large. The role of contaminating nonspecific surface and fiber seeds to this variation is well-understood.[7,14]

The designed β-solenoid protein scaffolds described here interact with both $IAPP_{20-29}$ and full-length IAPP, achieving solution- and cell-based effects that are far greater in magnitude than for the parent $gp5_{\beta f}$. This suggests we have met our goal of surface-based, sequence-specific interactions. However, for both solution biophysical and cell-based experiments, our observations were agonistic rather than antagonistic in nature. For $IAPP_{20-29}$ aggregation, one possibility is that the $gp5_{\beta f}$ templates succeed, as per our goal, in being coated by $IAPP_{20-29}$. Such coated templates would represent amyloid intersheet interface half-sites. Once formed, these could self-assemble into soluble, heterogeneously sized heteromeric aggregates, which we observe by light scatter, size exclusion chromatography, and electron microscopy. For cell-based toxicity with wild-type IAPP, our work with $gp5_{\beta f}$ molecules stands in marked contrast to that with BSA. BSA inhibits fiber formation but does not interfere with cellular toxicity.[9] In contrast, β-solenoid displaying $IAPP_{20-29}$ could interact with residues 20−29 present in the full-length protein. Such binding would have the effect of removing IAPP from its freely diffusing state, thereby preventing access to toxic conformations and/or the cell surface. In principle, these designed β-solenoid proteins could sequester as many as 24 copies of IAPP using the interaction based on residues 20−29. If this were to happen for full-length IAPP in cell culture, 0.5 μM $gp5_{NFAL}$ or $gp5_{NGIS}$ would all but eliminate the 13 μM IAPP used to induce toxicity. It is also possible that $gp5_{NFAL}$ and $gp5_{NGIS}$ catalyze the formation of nontoxic, off-pathway aggregated states of IAPP that then dissociate to regenerate the catalytic surface. A final possibility is that reduction of toxicity could be the result of $gp5_{\beta f}$ molecules inducing a cellular stress response that leads to upregulation of chaperones that target toxic IAPP aggregates for degradation. We do not favor the latter as the constructs on their own, under our conditions, do not show evidence of toxicity. Of the two former suggested possibilities, we favor the idea of peptide sequestration by the designed β-solenoids as it uses a single molecular description to provide an explanation for our solution biophysical and cell culture results.

The design principle described and executed here is an important addition to the set of tools that permit understanding of amyloid-based gains of function. In so doing, we join other efforts that have used molecular biology and/or synthetic chemistry approaches to lock short peptides into conformations that present β-strands.[29−31] Overall, these and our own tools have the potential to be leveraged to gain insights into processes relevant to pathology in disease as well as refining methods for controlled self-assembly of amyloid-based nanomaterials.

ASSOCIATED CONTENT

Supporting Information

CD spectra of $gp5_{\beta f}$ proteins, HPLC of soluble $IAPP_{20-29}/gp5_{\beta f}$ aggregates, and size exclusion assessment of $IAPP_{20-29}/gp5_{\beta f}$ aggregates. This material is available free of charge via the Internet at http://pubs.acs.org.

AUTHOR INFORMATION

Corresponding Author

*E-mail: andrew.miranker@yale.edu. Phone: (203) 432-8954. Fax: (203) 432-5175.

Funding

This work was funded by National Science Foundation (NSF) Grant 0907671, National Institutes of Health Grants RO1 GM102815 and T32GM007223, an NSF Graduate Research Fellowship to M.A.R., and an American Diabetes Association mentor-based postdoctoral fellowship to D.E.S.

Notes

The authors declare no competing financial interest.

ACKNOWLEDGMENTS

We thank Profs. S. Kanamaru and F. Arisaka (Tokyo Institute of Technology) for the gift of the gp5 gene and assistance with associated protocols and Profs. L. Regan, L. Rhoades, and A. Nath for critical reading of the manuscript.

DOI: 10.1021/bi5011442
Biochemistry 2015, 54, 987−993

■ ABBREVIATIONS

Aβ, amyloid β precursor from Alzheimer's disease; BSA, bovine serum albumin; DMSO, dimethyl sulfoxide; gp5, bacteriophage T4 cell-puncturing device β-helix; gp5$_{\beta\beta}$, bacteriophage T4 cell-puncturing device β-helix with foldon domain; gp5$_{NGIS}$, gp5$_{\beta f}$ mutated to present residues N-G-I-S on its surface; gp5$_{NFAL}$, gp5$_{\beta f}$ mutated to present residues N-F-A-L on its surface; GuHCl, guanidine hydrochloride; HPLC, high-performance liquid chromatography; IAPP, islet amyloid polypeptide; IAPP$_{20-29}$, peptide derived from islet amyloid polypeptide, residues 20−29; MRE, mean residue molar ellipticity; NMR, nuclear magnetic resonance; ThT, thioflavin T; TMS, tetramethylsilane; t_{50}, time at which 50% of the protein has converted to fiber.

■ REFERENCES

(1) Chiti, F., and Dobson, C. M. (2006) Protein Misfolding, Functional Amyloid, and Human Disease. *Annu. Rev. Biochem. 75*, 333−366.

(2) Fowler, D. M., Koulov, A. V., Alory-Jost, C., Marks, M. S., Balch, W. E., and Kelly, J. W. (2005) Functional amyloid formation within mammalian tissue. *PLoS Biol. 4*, e6.

(3) Soto, C. (2003) Unfolding the role of protein misfolding in neurodegenerative diseases. *Nat. Rev. Neurosci. 4*, 49−60.

(4) Münch, J., Rücker, E., Ständker, L., Adermann, K., Goffinet, C., Schindler, M., Wildum, S., Chinnadurai, R., Rajan, D., Specht, A., Giménez-Gallego, G., Sánchez, P. C., Fowler, D. M., Koulov, A., Kelly, J. W., Mothes, W., Grivel, J.-C., Margolis, L., Keppler, O. T., Forssmann, W.-G., and Kirchhoff, F. (2007) Semen-derived amyloid fibrils drastically enhance HIV infection. *Cell 131*, 1059−1071.

(5) Xu, J., Reumers, J., Couceiro, J. E. R., De Smet, F., Gallardo, R., Rudyak, S., Cornelis, A., Rozenski, J., Zwolinska, A., Marine, J.-C., Lambrechts, D., Suh, Y.-A., Rousseau, F., and Schymkowitz, J. (2011) Gain of function of mutant p53 by coaggregation with multiple tumor suppressors. *Nat. Chem. Biol. 7*, 285−295.

(6) Eisenberg, D., and Jucker, M. (2012) The amyloid state of proteins in human diseases. *Cell 148*, 1188−1203.

(7) Ruschak, A. M., and Miranker, A. D. (2007) Fiber-dependent amyloid formation as catalysis of an existing reaction pathway. *Proc. Natl. Acad. Sci. U.S.A. 104*, 12341−12346.

(8) Cohen, S. I., Linse, S., Luheshi, L. M., Hellstrand, E., White, D. A., Rajah, L., Otzen, D. E., Vendruscolo, M., Dobson, C. M., and Knowles, T. P. (2013) Proliferation of amyloid-β42 aggregates occurs through a secondary nucleation mechanism. *Proc. Natl. Acad. Sci. U.S.A. 110*, 9758−9763.

(9) Schlamadinger, D. E., and Miranker, A. D. (2014) Fiber-Dependent and -Independent Toxicity of Islet Amyloid Polypeptide. *Biophys. J. 107*, 2559−2566.

(10) Frieden, C. (2007) Protein aggregation processes: In search of the mechanism. *Protein Sci. 16*, 2334−2344.

(11) Magzoub, M., and Miranker, A. D. (2012) Concentration-dependent transitions govern the subcellular localization of islet amyloid polypeptide. *FASEB J. 26*, 1228−1238.

(12) Milojevic, J., Raditsis, A., and Melacini, G. (2009) Human serum albumin inhibits Aβ fibrillization through a "monomer-competitor" mechanism. *Biophys. J. 97*, 2585−2594.

(13) Milojevic, J., Costa, M., Ortiz, A. M., Jorquera, J. I., and Melacini, G. (2014) In vitro amyloid-β binding and inhibition of amyloid-β self-association by therapeutic albumin. *J. Alzheimer's Dis. 38*, 753−765.

(14) Hellstrand, E., Boland, B., Walsh, D. M., and Linse, S. (2010) Amyloid β-protein aggregation produces highly reproducible kinetic data and occurs by a two-phase process. *ACS Chem. Neurosci. 1*, 13−18.

(15) Madine, J., Jack, E., Stockley, P. G., Radford, S. E., Serpell, L. C., and Middleton, D. A. (2008) Structural insights into the polymorphism of amyloid-like fibrils formed by region 20−29 of amylin revealed by solid-state NMR and X-ray fiber diffraction. *J. Am. Chem. Soc. 130*, 14990−15001.

(16) Ruschak, A. M., and Miranker, A. D. (2009) The role of prefibrillar structures in the assembly of a peptide amyloid. *J. Mol. Biol. 393*, 214−226.

(17) Krampert, M., Bernhagen, J., Schmucker, J., Horn, A., Schmauder, A., Brunner, H., Voelter, W., and Kapurniotu, A. (2000) Amyloidogenicity of recombinant human pro-islet amyloid polypeptide (ProIAPP). *Chem. Biol. 7*, 855−871.

(18) Tenidis, K., Waldner, M., Bernhagen, J., Fischle, W., Bergmann, M., Weber, M., Merkle, M. L., Voelter, W., Brunner, H., and Kapurniotu, A. (2000) Identification of a penta- and hexapeptide of islet amyloid polypeptide (IAPP) with amyloidogenic and cytotoxic properties. *J. Mol. Biol. 295*, 1055−1071.

(19) Azriel, R., and Gazit, E. (2001) Analysis of the minimal amyloid-forming fragment of the islet amyloid polypeptide. An experimental support for the key role of the phenylalanine residue in amyloid formation. *J. Biol. Chem. 276*, 34156−34161.

(20) Kanamaru, S., Leiman, P. G., Kostyuchenko, V. A., Chipman, P. R., Mesyanzhinov, V. V., Arisaka, F., and Rossmann, M. G. (2002) Structure of the cell-puncturing device of bacteriophage T4. *Nature 415*, 553−557.

(21) Kanamaru, S., Gassner, N. C., Ye, N., Takeda, S., and Arisaka, F. (1999) The C-terminal fragment of the precursor tail lysozyme of bacteriophage T4 stays as a structural component of the baseplate after cleavage. *J. Bacteriol. 181*, 2739−2744.

(22) Yokoi, N., Inaba, H., Terauchi, M., Stieg, A. Z., Sanghamitra, N. J. M., Koshiyama, T., Yutani, K., Kanamaru, S., Arisaka, F., Hikage, T., Suzuki, A., Yamane, T., Gimzewski, J. K., Watanabe, Y., Kitagawa, S., and Ueno, T. (2010) Construction of Robust Bio-nanotubes using the Controlled Self-Assembly of Component Proteins of Bacteriophage T4. *Small 6*, 1873−1879.

(23) Tao, Y., Strelkov, S. V., Mesyanzhinov, V. V., and Rossmann, M. G. (1997) Structure of bacteriophage T4 fibritin: A segmented coiled coil and the role of the C-terminal domain. *Structure 5*, 789−798.

(24) Schlamadinger, D. E., and Miranker, A. D. (2014) Fiber-Dependent and -Independent Toxicity of Islet Amyloid Polypeptide. *Biophys. J. 107*, 2559−2566.

(25) Luca, S., Yau, W.-M., Leapman, R., and Tycko, R. (2007) Peptide conformation and supramolecular organization in amylin fibrils: Constraints from solid-state NMR. *Biochemistry 46*, 13505−13522.

(26) Bedrood, S., Li, Y., Isas, J. M., Hegde, B. G., Baxa, U., Haworth, I. S., and Langen, R. (2012) Fibril structure of human islet amyloid polypeptide. *J. Biol. Chem. 287*, 5235−5241.

(27) Huang, C.-J., Lin, C.-Y., Haataja, L., Gurlo, T., Butler, A. E., Rizza, R. A., and Butler, P. C. (2007) High Expression Rates of Human Islet Amyloid Polypeptide Induce Endoplasmic Reticulum Stress-Mediated β-Cell Apoptosis, a Characteristic of Humans with Type 2 but Not Type 1 Diabetes. *Diabetes 56*, 2016−2027.

(28) Cao, P., Tu, L.-H., Abedini, A., Levsh, O., Akter, R., Patsalo, V., Schmidt, A. M., and Raleigh, D. P. (2012) Sensitivity of Amyloid Formation by Human Islet Amyloid Polypeptide to Mutations at Residue 20. *J. Mol. Biol. 421*, 282−295.

(29) Khakshoor, O., and Nowick, J. S. (2009) Use of Disulfide "Staples" To Stabilize β-Sheet Quaternary Structure. *Org. Lett. 11*, 3000−3003.

(30) Gibbs, A. C., Kondejewski, L. H., Gronwald, W., Nip, A. M., Hodges, R. S., Sykes, B. D., and Wishart, D. S. (1998) Unusual β-sheet periodicity in small cyclic peptides. *Nat. Struct. Biol. 5*, 284−288.

(31) Cheng, P.-N., and Nowick, J. S. (2011) Giant Macrolactams Based on β-Sheet Peptides. *J. Org. Chem. 76*, 3166−3173.

DOI: 10.1021/bi5011442
Biochemistry 2015, 54, 987−993